Transition between Isotope-Mixing and Nonmixing States in Hydrogen-Deuterium Mixture Plasmas

Transition between isotope-mixing and non-mixing states in hydrogen-deuterium mixture plasmas

K.Ida,[1, 2] M.Nakata,[1, 2] K.Tanaka,[1] M.Yoshinuma,[1, 2] Y.Fujiwara,[1]
R.Sakamoto,[1, 2] G.Motojima,[1] S.Masuzaki,[1, 2] T.Kobayashi,[1, 2] and K.Yamasaki[3]

[1]*National Institute for Fusion Science, National Institutes of Natural Sciences, Toki, Gifu 509-5292, Japan*
[2]*SOKENDAI (The Graduate University for Advanced Studies), Toki, Gifu 509-5292, Japan*
[3]*Research Institute for Applied Mechanics Kyushu University, Kasuga, Fukuoka, Japan*
(Dated: December 14, 2019)

Transition between isotope-mixing and non-mixing states in hydrogen-deuterium mixture plasmas is observed in the isotope (hydrogen and deuterium) mixture plasma in Large Helical Device. In the non-mixing state, the isotope density ratio profile is non-uniform when the beam fueling isotope species differs from the recycling isotope species and the profile varies significantly depending on the ratio of the recycling isotope species, although the electron density profile shape is unchanged. The fast transition from non-mixing state to isotope-mixing state (nearly uniform profile of isotope ion density ratio) is observed associated with the change of electron density profile from peaked to hollow profile by the pellet injection near the plasma periphery. The transition from non-mixing to isotope-mixing state strongly correlates with the increase of turbulence measurements and the transition of turbulence state from TEM to ITG is predicted by gyrokinetic simulation.

Control of the isotope ratio in the plasma core is one of the crucial issues regarding fusion plasma, because the fusion power decreases as the deuterium-tritium (D-T) ratio in the core region deviates from 1:1. Although the isotope ratio of influx can be easily monitored by D_α and T_α lines, the individual isotope density has not been clarified whether the tritium density profiles are identical to the deuterium density profile. Although the isotope mixture plasma is necessary for this study, there are only a few experiments using the isotope mixture plasma [1, 2]. Hydrogen-deuterium (H-D) mixture plasma experiment in JET demonstrates that the H-D ratio profiles are insensitive to the isotope species of the recycling from the wall in the ITG dominant regime, where nearly uniform profile of the H-D ratio can be expressed as isotope-mixing state. Knowledge of the isotope state is limited due to a lack of precise measurements of isotope profiles. In many cases, the ion density profile shape, including the isotope-mixing state, is assumed to be identical to the electron density profile due to the quasi-neutrality. However, in the isotope mixture plasmas, the individually different isotope ion profiles are possible as long as the ambipolar condition is maintained, but the non-mixing state has never been observed experimentally so far. In recent work with gyrokinetic simulations, the non-mixing state is predicted in the TEM regime, while isotope-mixing state is predicted in the ITG regime [2]. There are also earlier works on the gyrokinetic simulations for the turbulent transport of the multiple isotope ions [3–5].

In this letter, we show a novel observation of evidence of the formation non-mixing profile and its transition to the isotope-mixing state in the plasma associated with the increase of turbulence level propagating in the ion diamagnetic direction. These results demonstrate that either of two isotope states (non-mixing or isotope-mixing) can exist in the H-D mixture plasma depending on turbulence state as predicted by the gyrokinetic simulations. Bulk charge exchange spectroscopy system [6–9] has been applied to measure the radial profiles of $n_H/(n_H + n_D)$ and $n_D/(n_H + n_D)$ in the plasma from H_α and D_α lines emitted by the charge exchange reaction between the bulk ions and the neutral beam injected in Large Helical Device (LHD) [10–12]. In order to study whether the ion particle transport is in the non-mixing state or the isotope-mixing state, the hydrogen and deuterium density profiles are measured in the plasmas with core hydrogen fueling by H-beam and edge deuterium fueling by recycling ($\Gamma_D > \Gamma_H$), where Γ_D and Γ_H are influx of deuterium and hydrogen evaluated with passive spectroscopy.

Figure 1 shows radial profiles of electron density normalized by the line-averaged electron density. The line-averaged electron density increases from 2 to $4 \times 10^{19} \text{m}^{-3}$ shot by shot due to increasing the hydrogen recycling, Γ_H/Γ_D, from 0.3 to 0.8. The electron density profile shapes are almost identical for these three discharges with different line-averaged density and different wall recycling isotope ratio. However, radial profile shapes of hydrogen and deuterium density are quite different depending on the ratio of hydrogen recycling. The amount of hydrogen density increases as the hydrogen recycling is increased, although the amount of deuterium density is similar for these three discharges. The increase of density is mainly due to the increase of hydrogen recycling from the wall. When the isotope recycling ratio is close to unity, there is almost no difference in profiles between hydrogen and deuterium as seen in Fig.1(b). In contrast, a significant difference in the profile shape (peaked or hollow) between hydrogen density and deuterium density is observed in the lower density plasma where the hy-
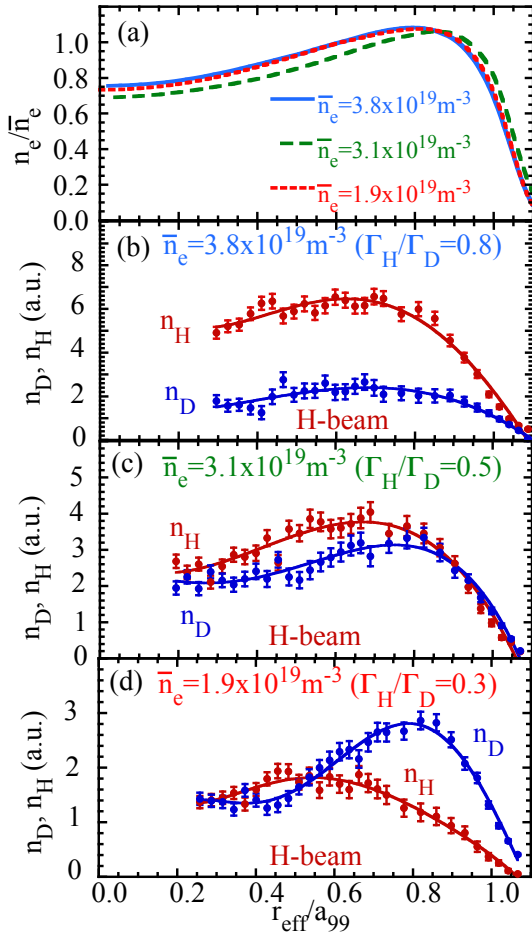
FIG. 1: (a) Radial profiles of electron density and (b)(c)(d) radial profiles of H and D density in the plasma with H-beam fueling for the different line-averaged density and wall recycling isotope ratio of (b) 3.8 $\times 10^{19}$m^{-3} ($\Gamma_H/\Gamma_D = 0.8$), (c) 3.1×10^{19}m^{-3} ($\Gamma_H/\Gamma_D= 0.5$), and (d) 1.9×10^{19}m^{-3} ($\Gamma_H/\Gamma_D = 0.3$).

drogen recycling is low enough ($\Gamma_H/\Gamma_D = 0.3$), as seen in Fig.1(d). These results clearly show the non-mixing state, where the isotope density profiles strongly depend on the location of the isotope source.

As seen in figure 2, the isotope fraction of bulk species, $n_H/(n_H + n_D)$ for H-beam and $n_D/(n_H + n_D)$ for D-beam, shows clear peaked profile when the isotope fraction of influx by wall recycling (indicated by arrows) is low. The isotope fraction at the LCFS ($r_{\rm eff}/a_{99}$ =1) decreases as the isotope fraction of influx is decreased. The hydrogen density is peaked in the plasma with hydrogen beam fueling and deuterium density is peaked in the plasma with deuterium beam fueling when the recycling of the beam species is low enough. In contrast, when the isotope fraction of beam species is close to 0.5 (the hydrogen influx is identical to the deuterium influx) the
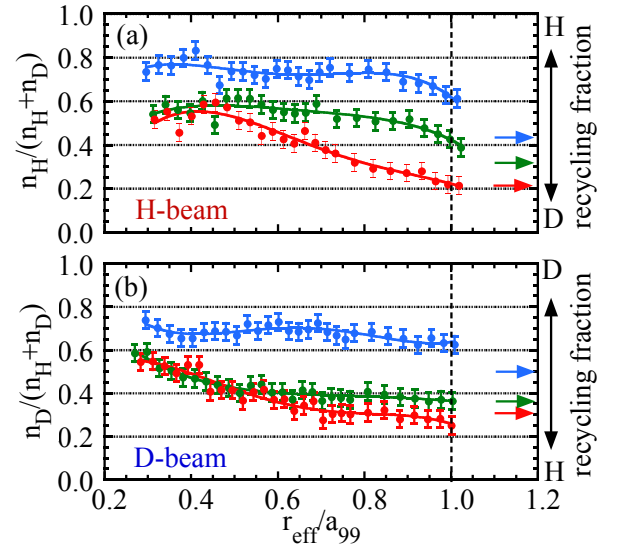

FIG. 2: Radial profiles of (a) hydrogen isotope fraction, $n_H/(n_H + n_D)$ with H-beam fueling and (b) deuterium isotope fraction, $n_D/(n_H + n_D)$ with D-beam fueling. The isotope fractions of recycling are indicated with arrows at the right y-axis.

isotope fraction profiles become flat. These results show clearly that the peaking of the isotope density is due to the fueling location rather than the transport difference between deuterium and hydrogen. Non-mixing state can be observed more clearly when the recycling of the beam fueling species is low enough (< 0.3).

The transition from non-mixing state to isotope-mixing state is observed after H and D pellet injections. The peak of the pellet deposition is $r_{\rm eff}/a_{99} \sim 0.9$ in these plasma conditions, which are evaluated experimentally from the increment of the electron density [15]. Because of the relatively shallow pellet deposition, pellet injections make the electron density profile more hollow. Figure 3 shows the change of radial profiles of H and D density by H-pellet and D-pellet injection in the target plasma with H-beam fueling and with low hydrogen recycling influx. After the H-pellet injection, the H density shows the significant increase, while the profile of D density is almost unchanged except for near the plasma periphery of $r_{\rm eff}/a_{99} > 0.85$. In contrast, the significant increase of H density as well as of D density is observed in the case of D pellet injection. This result indicates the fast redistribution of H density profile due to the additional fast transport process after the D pellet injection. Before the pellet injection the hydrogen density profile is much more peaked than the deuterium density profile due to the hydrogen beam fueling and deuterium dominant recycling. After the pellet injection the hydrogen density profile becomes similar in shape to deuterium density profile regardless of the species of pellet.

This change in the hydrogen and deuterium density
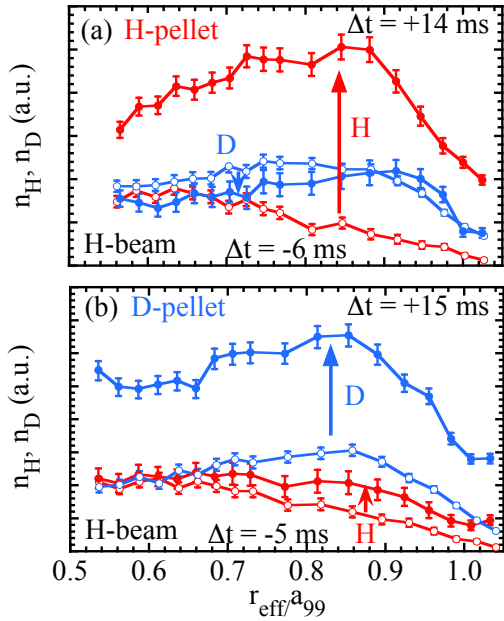
FIG. 3: Radial profiles of hydrogen (H) and deuterium (D) density in the plasma with H-beam fueling before ($\Delta t < 0$) and after ($\Delta t > 0$) (a) hydrogen pellet (#142315) and (b) deuterium pellet (#142314). The peak of deposition of pellets is located at $r_{\mathrm{eff}}/a_{99} \sim 0.9$.
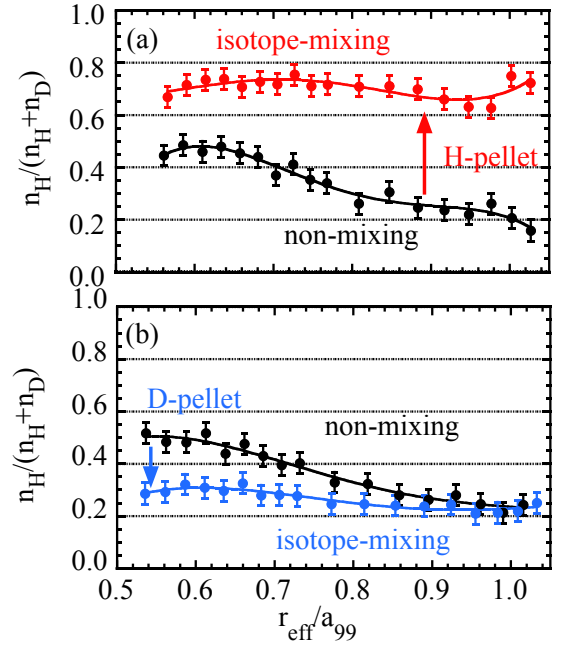

FIG. 4: Radial profiles of hydrogen isotope fraction, $n_H/(n_H + n_D)$ before and after the (a) H-pellet (#142315) and (b) D-pellet (#142314).

profile by the pellet injection demonstrates the change of states from non-mixing to isotope-mixing as clearly shown in the radial profile of isotope fraction in figure 4. Before the pellet injection, the hydrogen fraction profile is significantly peaked and the hydrogen fraction profile becomes flat after the hydrogen pellet near the plasma periphery. The flattening of hydrogen fraction profile is also observed in the deuterium pellet, although the peaking of hydrogen fraction profile is expected by the deposition of deuterium pellet. Therefore, the flattening of hydrogen fraction profile both for the hydrogen and the deuterium pellet is a clear evidence for isotope-mixing. If plasma is non-mixing state, the hydrogen fraction profile should be more peaked after the deuterium pellet injection because of the edge pellet deposition. The transition from non-mixing state to isotope-mixing state occurs in a shorter time (less than ~ 15 ms), which implies the large ion diffusion coefficient in the isotope-mixing state.

Figure 5 shows how the turbulence changes before (t=3.73sec) and after (t=3.77sec) pellet injection, which corresponds to the non-mixing and isotope-mixing states, respectively. Figure 5(a) shows the density fluctuation spectrum integrated from edge to core along the laser beam line of the central chord of phase contrast imaging (PCI) [16–18]. The wave number of the turbulence measured in this plasma is 0.2 - 0.4mm^{-1}. Both turbulence at high frequency (high phase velocity) and low frequency

(low phase velocity) increase by an order of magnitude in the isotope-mixing state. The radial profiles of poloidal rotation velocity measured with charge exchange spectroscopy are also over plotted in Fig.5(b)(c). Turbulence measured with PCI has $E \times B$ drift, the propagation direction with respect to the $E \times B$ drift is important to determine the type of the turbulence. The contour of density fluctuation in the space of normalized minor radius and phase velocity shows that there are two turbulence modes in the isotope-mixing state after the pellet injection. One is the turbulence propagating with $E \times B$ drift and the other is near edge turbulence propagating in the ion diamagnetic direction. The increase of turbulence and appearance of ion diamagnetic propagating turbulence is clearly observed associated with the transition from non-mixing and isotope-mixing states.

Figure 6(a)(b) shows the electron density, electron temperature, and ion temperature profiles for non-mixing and isotope-mixing states. Figure 6(c) shows the linear growth rates calculated with gyrokinetic simulation code GKV [19] for TEM and ITG turbulence, based on the radial profile of the density and the temperature measured. The non-mixing state is observed in the low-density plasmas ($n_e \sim 1.5 \times 10^{19}$m^{-3}) with electron cyclotron heating (ECH) and neutral beam injection (NBI), where the beam fueling isotope species differ from the isotope species due to recycling. Power of ECH is 2 MW and the power of NBI is 4.2 MW. The $n_H/(n_H + n_D)$ density profile is peaked for H beam fu-
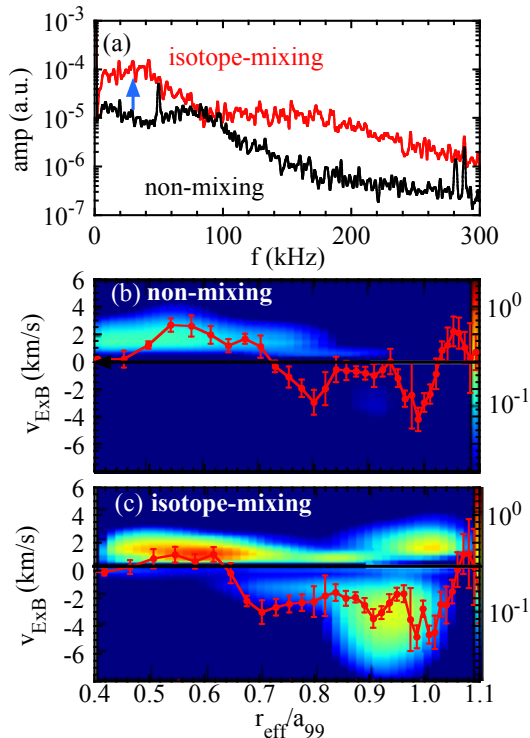
FIG. 5: (a) Density fluctuation spectrum in the non-mixing and isotope-mixing states in figure 4(a) and contour of density fluctuation in the space of normalized minor radius and phase velocity for (b) non-mixing state and (c) isotope-mixing state (#142315). Radial profiles of the projection of $V_{E\times B}$ to PCI observation plane are also plotted.
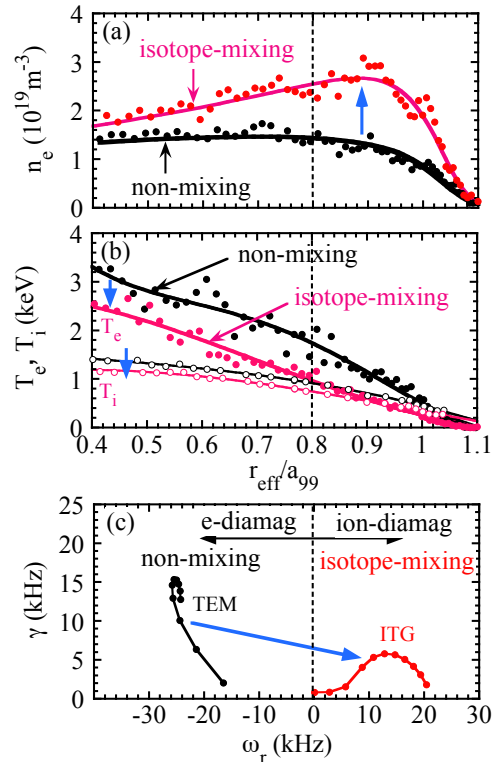

FIG. 6: Radial profile of (a) electron density and (b) electron and ion temperature before pellet injection (non-mixing state) and after pellet injection (isotope mixing state) and (c) the linear growth rate at $r_{\rm eff}/a_{99} = 0.8$ for the non-mixing and isotope-mixing states calculated with GKV.

eling and D recycling wall conditions. After the pellet injection, the isotope-mixing state is observed in higher density plasmas ($n_e \sim 2.5 \times 10^{19} {\rm m}^{-3}$). As seen in figure 6(b), electron temperature and its normalized gradient ($R_{\rm ax}/L_{T_e}$) decreases significantly but ion temperature decreases slightly. The ratio of electron temperature to ion temperature (T_e/T_i ratio) also decreases. Here, $R_{\rm ax}$ is a major radius of magnetic axis and L_{T_e} and L_{T_i} are the inverse of logarithmic gradients, $(\partial \ln T_e/\partial r)^{-1}$ and $(\partial \ln T_i/\partial r)^{-1}$, respectively. The T_e/T_i ratio and the normalized T_e gradient ($R_{\rm ax}/L_{T_e}$) at $r_{\rm eff}/a_{99} = 0.8$ decreases from 1.73 to 1.30 and from 19.3 to 11.6, respectively, while the normalized T_i gradient ($R_{\rm ax}/L_{T_i}$) increases slightly from 11.1 to 13.8. The impact of the collisionality in isotope plasmas and the sign of the density gradient on TEM and ITG mode is studied in LHD using gyrokinetic simulation [20–22]. When the sign of density gradient changes from negative ($\partial n_e/\partial r$ (0.8) < 0 : peaked) to positive ($\partial n_e/\partial r$ (0.8) > 0 : hollow), the growth rates of both TEM and ITG decrease. The gyrokinetic simulation predicts that TEM propagating in the electron diamagnetic direction is unstable for the non-mixing state. However, the TEM is stabilized and ITG mode propagating in the ion-diamagnetic direction

becomes unstable for the isotope-mixing state. The mode transition from TEM to ITG mode is due to the decrease of T_e/Ti ratio, increase of collisionality (n_e rise and T_e drop), and sign flip of the electron density gradient from negative (peaked profile) to positive (hollow profile).

Effective diffusion coefficient of particle transport, $D_s = -\Gamma_s^{(GK)}/(\partial n_s/\partial r)$, for ion ($s$=i) and for electron ($s$=e) are evaluated from the quasi-linear approximation in the gyrokinetic calculations. The ratio of ion diffusion to electron diffusion coefficient, D_i/D_e, is 0.4 for the case of TEM dominant state before the pellet injection, while D_i/D_e is 2.5 for the case of ITG-dominant state after the pellet injection. When the electron particle diffusion is dominant $D_e > D_i$, the radial profile of each isotope species can differ depending on the source location of each species (non-mixing state). In contrast, when the ion particle diffusion is dominant $D_i > D_e$, the radial profile of each isotope species becomes identical due to the large diffusion (isotope-mixing state). The electron and ion diffusion coefficient evaluated from the quasi-linear gyrokinetic calculations well reproduces the qualitative tendency of the non-mixing and isotope-mixing states observed in the experiment. Although non-

linear gyrokinetic simulation for multiple ion species in LHD plasmas is numerically challenging, the systematic investigations of correlations among the turbulent particle transport levels, its direction, and the driving micro-instabilities are useful for more quantitative comparisons with the above experimental results. Also, the gyrokinetic simulations for the transient phase, which will remain as future works, can clarify the threshold between the isotope-mixing and the non-mixing states. The non-linear turbulence simulations, which are important for making quantitative comparisons, will be addressed in future.

In conclusion, both the non-mixing and the isotope-mixing states are observed in the hydrogen-deuterium mixture plasma in LHD. The non-mixing state is observed in the slightly peaked density plasma with low recycling beam fueled plasma and the isotope fraction profiles depend on the location of the isotope source (core beam fueling or edge influx due to recycling). The isotope-mixing state is observed in the hollow density plasma after the pellet injection and the isotope fraction profile becomes flat regardless of the location of the isotope source. This paper reports important findings on non-mixing state between hydrogen and deuterium ions in the H-D mixture plasma. This finding implies that non-mixing state between deuterium and tritium ions could be also achieved in the D-T mixture plasma in JET and ITER depending on the turbulence state and gives insight for controlling the isotope ratio profile in future fusion devices.

---

[1] P.C. Efthimion, L. C. Johnson, J. D. Strachan, E.J. Synakowski, M. Zarnstorff, H. Adler, C. Barnes, R. V. Budny, F.C. Jobes, M. Louglin, D. McCune, D. Mueller, A. T. Ramsey, G. Rewoldt, A. L. Roquemore, W. M. Tang, and G. Taylor, *Phys. Rev. Lett.* **75** 85 (1995).

[2] C. Bourdelle, Y. Camenen, J. Citrin, M. Marin, F.J. Casson, F. Koechl, M. Maslov and The JET Contributors, *Nucl. Fusion* **58** 076028 (2018).

[3] C. Estrada-Mila, J. Candy, and R. E. Waltz, *Phys. Plasmas* **12**, 022305 (2005).

[4] I. Pusztai, J. Candy, and P. Gohil, *Phys. Plasmas* **18**, 122501 (2011).

[5] M. Nakata, M. Honda, M. Nunami, T.-H. Watanabe, and H. Sugama, Multi-species ITG-TEM driven turbulent transport of D-T ions and He-ash in ITER burning plasmas, *Preprint: 2016 IAEA Fusion Energy Conference, (Kyoto, Japan, 17-22 October 2016)* [TH/P2-2] https://www-pub.iaea.org/iaeameetings/48315/26th-IAEA-Fusion-Energy-Conference.

[6] B.A. Grierson, K. H. Burrell, C. Chrystal, R. J. Groebner, D. H. Kaplan, W.W. Heidbrink, J.M.Munoz Burgos, N. A. Pablant, W.M. Solomon, M.A. Van Zeeland *Rev. Sci. Instrum.* **83**, 10D529 (2012).

[7] S.R. Haskey, B.A. Grierson, K.H. Burrell, C. Chrystal, R.J. Groebner, D.H. Kaplan, N.A. Pablant, and L. Stagner, *Rev. Sci. Instrum.* **87**, 11E553 (2016).

[8] S.R. Haskey, B.A. Grierson, L. Stagner, C. Chrystal, A. Ashourvan, A. Bortolon, M.D. Boyer, K.H. Burrell, C. Collins, R.J. Groebner, D.H. Kaplan, N.A. Pablent *Rev. Sci. Instrum.* **89**, 10D110 (2018).

[9] S.R. Haskey, B.A. Grierson, C. Chrystal, A. Ashourvan, K.H. Burrell, R.J. Groebner, E.A. Belli, L. Stagner, D.J. Battaglia, T. Stoltzfus-Dueck, A. Bortolon *Plasma Phys. Control Fusion* **60** 105001 (2018).

[10] K. Yamasaki, K. Ida, M. Yoshinuma, T. Kobayashi, *Plasma. Fusion. Res.* **13**, 1202103 (2018).

[11] K. Ida, M. Yoshinuma, T. Kobayashi, Y. Fujiwara, J. Chen, I. Murakami, M. Kisaki, M. Osakabe, *Plasma. Fusion. Res.* **14**, 1402079 (2019).

[12] K. Ida, M. Yoshinuma, K. Yamasaki, T. Kobayashi, Y. Fujiwara, J. Chen, I. Murakami, S. Satake, Y. Yamamoto, S. Murakami, M. Kobayashi, *Rev. Sci. Instrum.* **90**, 093503 (2019).

[13] M. Yoshinuma, K. Ida, M. Yokoyama, M. Osakabe, K. Nagaoka, *Fusion Sci. Technol.* **58**, 375 (2010).

[14] J. Chen, K. Ida, M. Yoshinuma, I. Murakami, T. Kobayashi, M.Y. Ye, B. Lyu *Phys. Lett. A* **383** 1293 (2019).

[15] K. Ida, *et. al.*, *Nucl. Fusion* **59**, 056029 (2019).

[16] K. Tanaka, C. A. Michael, L. N. Vyacheslavov, A. L. Sanin, K. Kawahata, T. Akiyama, T. Tokuzawa, and S. Okajima *Rev. Sci. Instrum.* **79** 10E702 (2008).

[17] C. A. Michael, K. Tanaka, L. Vyacheslavov, A. Sanin, and K. Kawahata *Rev. Sci. Instrum.* **86** 093503 (2015).

[18] K. Tanaka, *et. al.*, *Nucl. Fusion* **57**, 116005 (2017).

[19] T.-H. Watanabe and H. Sugama, *Nucl. Fusion* **46**, 24 (2006).

[20] M. Nakata, M. Nunami, H. Sugama, and T.-H. Watanabe, *Plasma Phys. Control. Fusion* **58**, 074008 (2016).

[21] M. Nakata, M. Nunami, H. Sugama, and T.-H. Watanabe *Phys. Rev. Lett.* **118** 0165002 (2017).

[22] M. Nakata, K. Nagaoka, K. Tanaka, H. Takahashi, M. Nunami, S. Satake, M. Yokoyama, F. Warmer *Plasma Phys. Control. Fusion* **61** 014016 (2019).